Review Article on Advanced Imaging in The Diagnosis of Cardiovascular Diseases

4D flow imaging of the thoracic aorta: is there an added clinical value?

Federica Catapano[1], Giacomo Pambianchi[1], Giulia Cundari[1], João Rebelo[2], Francesco Cilia[1], Iacopo Carbone[1], Carlo Catalano[1], Marco Francone[1], Nicola Galea[1,3]

[1]Department of Radiological, Oncological and Pathological Sciences, Sapienza University of Rome, Rome, Italy; [2]Department of Radiology, Centro Hospitalar São João, Alameda Prof. Hernâni Monteiro, Porto, Portugal; [3]Department of Experimental Medicine, Sapienza University of Rome, Rome, Italy

Contributions: (I) Conception and design: N Galea, M Francone; (II) Administrative support: I Carbone, C Catalano; (III) Provision of study materials or patients: F Catapano, G Pambianchi, G Cundari, F Cilia, N Galea, I Carbone, M Francone; (IV) Collection and assembly of data: F Catapano, G Pambianchi, G Cundari, F Cilia, N Galea; (V) Data analysis and interpretation: F Catapano, G Pambianchi, G Cundari, F Cilia, N Galea; (VI) Manuscript writing: All authors; (VII) Final approval of manuscript: All authors.

Correspondence to: Dr. Nicola Galea, MD PhD. Department of Experimental Medicine, "Sapienza" University of Rome, viale Regina Elena 324, 00161 Rome, Italy. Email: nicola.galea@uniroma1.it.

Abstract: Four-dimensional (4D) flow MRI has emerged as a powerful non-invasive technique in cardiovascular imaging, enabling to analyse in vivo complex flow dynamics models by quantifying flow parameters and derived features. Deep knowledge of aortic flow dynamics is fundamental to better understand how abnormal flow patterns may promote or worsen vascular diseases. In the perspective of an increasingly personalized and preventive medicine, growing interest is focused on identifying those quantitative functional features which are early predictive markers of pathological evolution. The thoracic aorta and its spectrum of diseases, as the first area of application and development of 4D flow MRI and supported by an extensive experimental validation, represents the ideal model to introduce this technique into daily clinical practice. The purpose of this review is to describe the impact of 4D flow MRI in the assessment of the thoracic aorta and its most common affecting diseases, providing an overview of the actual clinical applications and describing the potential role of derived advanced hemodynamic measures in tailoring follow-up and treatment.

Keywords: Four-dimensional flow imaging (4D flow imaging); phase contrast sequence; cardiovascular magnetic resonance; thoracic aorta; fluid dynamics

Submitted Apr 24, 2020. Accepted for publication Jun 10, 2020.
doi: 10.21037/cdt-20-452
View this article at: http://dx.doi.org/10.21037/cdt-20-452

Introduction

More than two decades after its introduction, four-dimensional flow magnetic resonance imaging (4D flow MRI) has been established as an unrivaled method for the non-invasive in vivo assessment of fluid dynamics.

The reference technique of 4D flow MRI is a three-dimensional (3D) phase contrast sequence with three-directional velocity encoding, which has been widely implemented over the years and nowadays offers high reproducibility and robustness.

Although the development of this technique required a long time due to the heterogenity of technical strategies proposed, intrinsic difficulties in reproducibility and of the complex processing of such a large amount of data, today 4D flow MRI is widely available and many analysis softwares are commercially available for clinical validation.

A number of studies (and clinical trials) have been conducted over the years and are still ongoing to explore the application of 4D flow MRI in many different areas of

Table 1 VENC ranges in thoracic aorta

Study region and setting	VENC (cm/sec)
Normal thoracic aorta	100–200
Aortic stenosis	200–400
Aortic aneurism/dilation	100

VENC, velocity encoding.

cardiovascular system and to define its actual additional value.

In particular, research interests are mainly oriented in extrapolating quantitative flow data and related energy parameters that may emerge as clinical biomarkers to improve early diagnostics and prognostic prediction.

This review aims to shed light on state of the art of 4D flow MRI in the clinical assessment of a large spectrum of pathological conditions affecting the thoracic aorta and to give useful elements for its immediate introduction in daily clinical routine.

Technique

The 3D Phase Contrast sequence, also known as 'flow-sensitive' or 'velocity mapping', is the technique typically used in 4D-flow MRI consisting in a short TE (5–7 ms) and TR (2–4 ms) radiofrequency-spoiled gradient-echo. It allows for a rapid imaging of the vessels flow in absence of contrast agent administration; however a recent study concluded that the echoplanar imaging (EPI) sequence produces higher data quality (1,2).

Even if the contrast agent administration is not necessary in 4D flow MRI, the sequence acquisition after gadolinium improves the contrast between the blood and the surrounding tissues, resulting in a better signal-to-noise ratio and velocity-to-noise ratio (1).

In order to depict even the subtle changes in flow a high spatial resolution (isotropic voxel size: 1.5–3.0 mm for the aorta) is fundamental, whereas the highest possible temporal resolution, (generally <40 ms; preferably ≥20 phases) enables to catch even the rapid flow phenomena (3,4).

The maximum velocity encoding (VENC) value to set before starting the 4D flow MRI sequence acquisition is typically around 150 ms (*Table 1*), even though this value should be increased in the presence of flow accelerations (e.g., valve stenosis, coarctation) to avoid aliasing artifacts.

As for the 2D-PC MRI, the quality of velocity images can be degraded by noise. The velocity noise, in this kind of imaging, is directly proportional to the Venc preset value, but inversely related to the signal-to-noise ratio (SNR) in the corresponding magnitude images (i.e., vnoise is proportional to Venc/SNR) (5).

It should be kept in mind that an increase in the Venc values is needed to avoid aliasing, but at the same time, keeping the Venc as low as possible will reduce velocity noise and improve image quality (5,6). The best compromise should be found in each patient.

Therefore, it is advisable that the set VENC value should be approximately 10% higher than the registered maximum velocity (7).

When the maximum velocity of aortic flow is unknown or not conceivable, a solution may be to acquire one or more bidimentional phase contrast sequences (2D PC MRI) in the regions of stenosis identified on the MR angiography or cine images. Another promising approach is the use of a multi-velocity encoding (multi-VENC) that additionally improves pathline tracking and streamline estimation (8).

A structured workflow is suggested as shown below.

Patient preparation

Cardiovascular MRI exams are usually time-consuming (40–50 min) and 4D flow MRI further extends the exam duration, it is therefore essential to inform the patient in advance for the maximum compliance as well as to reduce patient discomfort.

Retrospective gating is preferable in order to cover the entire ECG cycle and avoid interrupting the sequence. However, in the presence of irregular heart rate (e.g., atrial fibrillation, ventricular bigemism or frequent ventricular extrasystoles), common cause of blurred images, prospective gating should be used, as it is less susceptible to cardiac movement artefacts (6).

ECG retrospective triggering with a clearly detectable R-wave trace is fundamental in 4D flow MRI to ensure the consistency between RR-intervals, recognition of the cardiac cycle phases and appropriate image quality (7).

The surface multi-channel body coil should be positioned to encompass the entire thoracic volume, as the aortic arch can extend to or above the level of the medial ends of the clavicles.

Image acquisition

Due to the large amount of data, the number of acquired slides should always be limited to the coverage of the flow

region to be studied. Regardless, the acquisition time for the thoracic aorta using an ECG and a respiratory gating is generally 10–15 min.

Besides the patient-dependent factors, the scanning time is basically determined by spatial/temporal resolution and anatomical volume coverage.

Phased-array coils, multi-receiver channels, and parallel imaging are mandatory to maintain scan duration within an acceptable range.

Several k-space based techniques have been proposed to accelerate data acquisition in 4D-flow imaging and reduce scan time:

- k-t-undersampling;
- Segmented k-space filling;
- Parallel imaging like in: SENSE (SENSitivity Encoding), SMASH (simultaneous acquisition of spatial harmonics), GRAPPA (GeneRalized Autocalibrating Partial Parallel Acquisition) and k-t GRAPPA.

A combination of these approaches allows the visualization of the entire aorta in less than 5 min (depending on the volume covered) (9), or even less than 2 min (10).

Alternative powerful techniques make use of non-Cartesian data sampling strategies, such as vastly undersampled isotropic voxel radial projection imaging (PC-VIPR), which benefit from insensitivity to the patient's movement, or spiral k-space sampling. On the other hand, these strategies are sensitive to eddy currents effects and require more demanding calculation power (6).

Compressed sensing has also demonstrated to be a promising acquisition accelerating technique, capable of shortening the scan times to around 2–3 min without substantial degradation of the image quality in aortic 4D flow MRI. This could be a significant improvement especially for patients who cannot stay still in the scanner gantry for a long time (i.e. pediatric population) (11).

Image pre-processing:

The 4D flow MRI raw data generally contains many errors; the main ones being:

- Maxwell terms, that result in spatially varying phase offsets;
- Eddy currents, caused by the quick switching on/off of the magnetic field gradients;
- Phase-wrapping artifacts;
- Gradient field distortions;
- Aliasing artefacts.

These errors should be corrected to enhance the image quality and the consistency of acquired data. A variety of continuously updating approaches are being developed by different vendors in order to filter and compensate/offset these inaccuracies. In particular, for the aliasing artefacts, a phase unwrapping algorithm is currently a valid current solution incorporated in many built-in analysis softwares.

Another source of artifacts is obviously the patient's movement, which unfortunately cannot be corrected after acquisition. The application of respiratory triggering and an adequate preparation of the patient instructing them on limiting body movements and respiratory excursions are necessary to optimize the acquired images (*Figure 1*).

In order to minimize breathing motion artifacts, 4D flow MRI sequences is often acquired in combination with respiratory gating, using bellows, self-gating, or a navigator gating. Respiratory gating strategies were originally developed for coronary MRA, and then typically used in 4D flow MRI in order to avoid long apneas, thus extending availability to a wider group of patients (12). Unfortunately, this approach further increases the total scan time and makes the sequence more susceptible to body motion artifacts.

The current consensus recommend leading or trailing MR navigator gating on liver/diaphragm interface, when available, using a 6 mm window size, which results in 50% scan efficiency; even if a 100% acceptance rate with a motion correction would be ideal, it is too much too demanding in terms of scan time (1).

However, many authors have described free-breathing 4D flow MRI without respiratory gating (13), with shorter acquisition times, and the debate about its applicability is still ongoing.

Segmentation

Once the four volumetric "time resolved" image datasets have been loaded (1 magnitude depicting anatomy and 3 velocity encoded according to the three orthogonal encoding directions x, y, and z), an anatomical segmentation of the entire thoracic aorta is necessary to suppress background signal. This process is usually applied on the magnitude images since they are the best images to differentiate the static tissue from the blood flow within the aortic lumen and often an automatic or semiautomated tool is embodied within the software analysis.

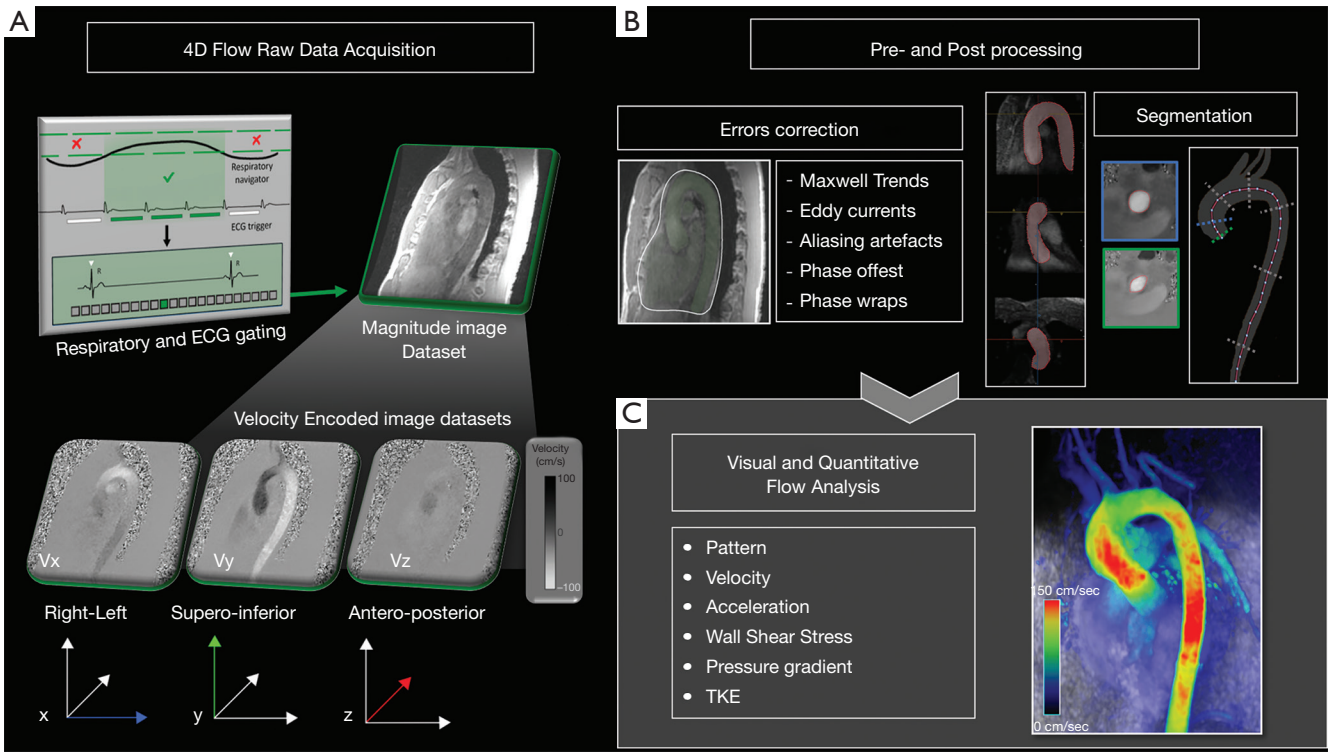

Figure 1 DATA acquisition and processing. (A) In order to reconstruct 4D volumetric data sets, volumetric magnitude data and three phase-difference volumes, encoded in the three directions of space (x, y, z), are acquired. (B) Raw data are preprocessed. 4D flow data are affected by systematic velocity encoding errors caused by magnetic field inhomogeneity, concomitant magnetic fields (Maxwell terms), and eddy currents. Data pre-processing is a crucial moment during data analysis workflow: background phase-offset errors or aliasing artefacts may compromise the flow visualization and quantification, so is fundamental to correct them before the analysis step. (C) Finally, it's time of visual and quantitative analysis of the images.

Image analysis

Imaging analysis needs to be supported by ad hoc software that allows the interactive and fully retrospective 3D flow evaluations. It relies on three-dimensional visualization of streamlines, path-lines or vector fields encoded using colorimetric scale and, when available, the calculation of derived flow features.

In particular, streamlines represent instantaneous blood flow vector field through a 3D velocity field, tangent to the velocity vectors at a specific point in time and provide an overview of spatial distribution and orientation of blood flow velocities.

However, they are not able to represent the temporal evolution of the blood flow velocity data. This role is entrusted to the path-lines, which are the time-resolved trajectories that fluid particles follow through the dynamic velocity field during a cardiac cycle, able to give us dynamic information about the blood flow pattern (1).

On the visual assessment, different flow components can be distinguished:

- Helical flow: the particles move in a spiral producing helical streamlines. Initial jet flow may be eccentric, with high-velocity flows near the vessel wall.
- Vortical flow: the particles make rotations in the flow field, with streamlines that draw a whirlpool-like flow pattern. Some conditions, such as aortic aneurysms and valvulopathies, are correlated with the presence and the intensity of vortex flows (14,15).

Vectors simultaneously at the same time the speed and direction of flow with an arrow calculated from the magnitudes of the vectoral components of velocity (*Figure 2*).

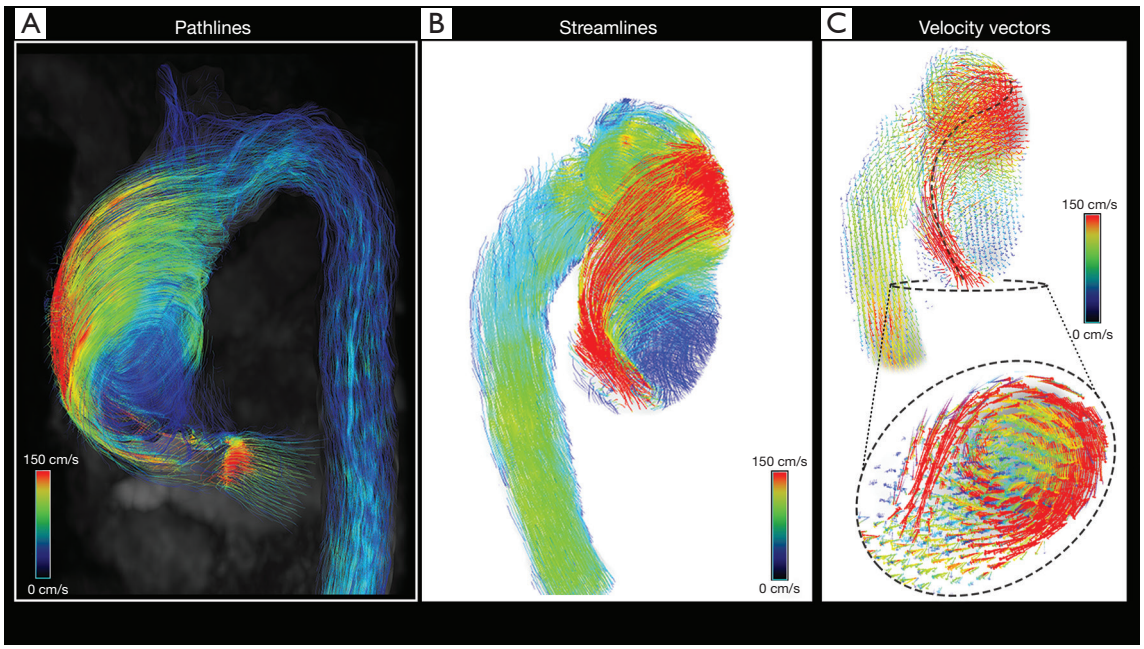

Figure 2 Colour-encoded thoracic aorta flow visualization modalities. Time-resolved path-lines (A) show the trajectories of fluid particles during a systolic peak in a dilated aorta, drawing a big vortex into the aneurism. Eccentric systolic jet in red, represented by the 3D streamlines (B) and velocity vectors (C), principally arranged along the right-anterior wall of the ascending aorta. The flow subsequently turns clockwise to the left and upwards, showing high degree of vorticity, until it reaches the aortic arch. In the transversal view, from the bottom to the top of the ascending aorta (C, on the bottom), the vectors clearly display the clockwise rotation of the flow into the aneurysm.

Quantitative assessment

The first approach is to assess the flow passing through an analysis plane transversely oriented to the long axis of the vessel and positioned in the section of interest.

Flow velocity (mean and peak velocity), flow acceleration and flow rate can be retrospectively measured setting cross-sectional bidimensional planes in any spatial orientation.

These planes are also employed to generate 3D streamlines or time-resolved 3D pathlines for geometric flow pattern visualization, which represent traces along the instantaneous 3D blood flow velocity vector field for any individual cardiac time-frame.

Derived flow parameters extrapolation may integrate the flow analysis with the assessment of those features related to flow energy and dependent from the interaction between flow and vessel wall:

- Laminar flow: assessed by the predominance or less of particles movement parallel to the major axis of the vessel (according to Reynolds number).
- Flow jet angle: the angle between the mean vector extrapolated from the peak systolic jet and the normal to the transverse cross-sectional plane passing through the vessel (16).
- Flow displacement: the distance between the center of the vessel lumen and the "center of velocity" of the forward flow; the distance should be normalized to the vessel transverse diameter; it is the parameter which better describes the flow eccentricity (16).
- In-plane rotational flow: is a fluid-dynamics parameter used to quantify rotation tendency of blood flow within a cross-sectional plane, also defined as the through-plane component of the circulation (17).
- Wall shear stress (WSS) and its vectorial components (axial, circumferential): is the shear force generated by the blood stream acting on the vessel wall, considered one of the main factors in development and progression of aortopathy, as its values and distribution are directly correlated to atherosclerosis (18), the extracellular matrix dysregulation and elastic fibers degeneration (19).
- Turbulent kinetic energy (TKE): the energy stored in turbulent flow, widely dissipated into heat. It

measures the blood flow turbulence intensity, in a direction-independent way and expresses the rapid velocity fluctuations within a single imaging voxel (6,20). TKE also correlates with irreversible pressure loss within the vessel, as indirect markers of blood flow efficiency (21).

- Viscous energy loss: this parameter measures the conversion of nonturbulent mechanical energy into thermal energy per volume units; it's based on the concept of viscous dissipation and can be calculated using a reformulation of the viscous portion of the Navier-Stokes energy equations (6,22). Viscous energy losses are not related to turbulence however to a lesser extent, can contribute in quantifying energetic losses in patients with aortic dilation and aortic valve disease (22,23).
- Pressure gradient: a useful biomarker for evaluating vessel stenosis (e.g., in the aortic coarctation or in valve stenosis). The colorimetric map shows the pressure modification and distribution in the vessel during the cardiac cycle (24).
- Pulse wave velocity: the most useful indicator of vessel wall elasticity and stiffness. The pulse wave velocity through the aorta should always be measured with a temporal resolution <40 ms (25,26).

Normal aorta

The simple visual assessment (5) of the flow streamlines in the normal thoracic aorta reveals the "candy-cane" flow geometry with the highest velocities in central areas and lower in the peripheral zone, as hypothesized by Newton and Bernoulli (17th and 18th century).

The flow velocity is greatest in both the ascending and descending aorta, while decreased in the transverse aorta, where the arcuate morphology converts the parallel direction of the flow into angular motion.

In normal subjects with a tricuspid valve the valve jetflow at the aortic root is predominantly laminar, which minimizes the friction with the vessel wall and results in a homogeneous distribution of WSS perpendicular to an axial slice through the vessel and parallel to the vessel wall (in laminar flow the WSSax is the dominating vector of WSS) (27).

Hope *et al*. (28) performed 4D-flow on 19 healthy volunteers and demonstrated that normal aortic flow progresses with an initial jet towards the anterior right wall of the ascending aorta (AscAo) which bends posterolaterally towards the inner curvature creating two opposing helices, one right-handed (or "clockwise" vortex) helix along the left wall and one left-handed ("counterclockwise" vortex) along the right wall. In most volunteers the right-handed helix is larger than the left-handed one (nearly 80% of healthy volunteers); between the two helices the occurrence of a retrograde flow is seen along the inner curvature in all volunteers, which is known to contribute to coronary perfusion (29). In the helical flow the WSS is predominantly circumferential (WSScirc), which is parallel to the vessel wall circumference.

Burk *et al*. (30) showed that normal helix flow occurring in AscAo during the ventricular systole has a flow rotation typically <180°, and greater vortex forces are significantly associated with dilatated AscAo.

Helix and vortex flow were observed less frequently in the aortic arch and descending aorta (DesAo) than in AscAo both in controls and in patients with dilatated AscAo.

4D flow MRI (31) of normal aortic root not only confirmed the vortex formation of retrograde flow in diastolic phase, but also enables us to verify what was brilliantly theorized in the sixteenth century by Leonardo Da Vinci about vortex generation in the sinus of Valsalva: "the effect of this revolution of the blood is to shut again the open valve of the heart making by its primary reflected motion a perfect closure" (Quadr. Anat. IV, fol. 11 r).

The early systolic vortex flow patterns forming in the three sinuses of Valsalva in normal aorta modulate the movement of the aortic leaflets during the progressive closure of the aortic valve.

The vortexes persist into early diastole with a rotational direction from superior to inferior along the external margins of the sinuses, then turning toward the central aortic orifice, by exerting an inward pressure on the aortic leaflets and ensuring synchronous and stress-free valve closure (32).

Aortic valve stenosis (AS)

AS is the most frequent valvular heart disease in developed countries and consists in leaflet opening impairment secondary to congenital or acquired abnormalities, often associated to development of aortic root dilatation and LV hypertrophy (33).

The mechanisms of stenosis-induced aortic dilatation have been presumed to be flow-related, and various studies have been focused on identifying hemodynamic markers that may trigger maladaptive vascular remodelling, leading

to specific shape and dilatation phenotype and that can be used to predict disease progression (34,35).

The exploration of the relationships between the abnormality of valve morphology, modifications in aortic flow patterns and the associated aortopathy could offer new perspectives into improved prognostic stratification and tailoring therapeutic approaches.

Diagnosis and staging of AS is commonly achieved by transthoracic echocardiography (TTE), which allows for accurate measurements of peak jet velocity (Vpeak), mean pressure gradient (Pmean), aortic valve area (AVA) and left ventricular function (LVEF) (7,36).

Current criteria for severe AS include mean transvalvular pressure gradient ≥40 mmHg, peak aortic jet velocity ≥4 m/s or indexed aortic valve area (AVA) <0.6 cm^2/m^2 (37).

However, TTE has some limitations, such as inadequate images due to patient characteristics, risk for misalignment of the ultrasound beam with the AS jet in presence of flow eccentricity and/or angulation, that may lead to an underestimation of peak aortic jet velocity and mean pressure gradient in AS patients (37).

Moreover, approximately one-third of patients with severe AS has discordant echocardiographic findings, such as small AVA but non-severe mean pressure gradient, and often requires additional imaging assessment (38).

MRI is a valid alternative in measuring the transvalvular peak velocity enabling the non-invasive indirect estimation of the pressure gradient. However, the misplacement of the valve plane during the scanning can lead to an incorrect quantification of peak velocity.

In comparison with 2D PC MRI, 4D flow MRI is more accurate for measuring inlet or outlet valve flow, because it allows us to adapt the valve analysis plane to the inherently movement along the longitudinal axis during the cardiac cycle (39,40).

Furthermore, 4D flow MRI is not hampered by flow eccentricity, since its multidirectional velocity-encoding enables the post-hoc quantification of velocities regardless of the spatial orientation of the flow jet, and may be integrated by the assessment of flow-derived parameters, such as WSS, pressure gradients, and TKE (33) (*Figure 3*).

Irreversible pressure loss caused by energy dissipation in post-stenotic flow is a marker used to assess hemodynamic significance of aortic stenosis which may provide independent and additional prognostic information in asymptomatic AS patients (41), as an increase in the energy loss results in an increased LV workload to preserve the cardiac output (39).

The gold standard in measuring irreversible pressure loss (net transvalvular pressure gradient, TPGnet) is catheterization, but this is rarely used due to its invasiveness (20).

Therefore, this value is generally indirectly estimated by echocardiography using the Bernoulli equation. The main constraints of this technique are the assumption that the flow is always laminar (without turbulence) (39) and it neglects the viscous energy dissipation (39).

4D flow MRI measures the irreversible pressure loss by the flow-derived TKE (energy loss by turbulent flow), which considers the velocity fluctuations within each imaged voxel and thus reflects the amount of energy dissipation through the stenosis (41).

Dyverfeldt *et al*. demonstrated that the peak total TKE in the AS patients was significantly higher than in the normal volunteers (P<0.001) and that total TKE was strongly correlated with irreversible pressure loss (R^2=0.91) (20).

Therefore, 4D flow-derived TKE can provide complementary information when compared with TTE for the determination of AS severity, and could be used as a valuable alternative in the non-invasive measurement of irreversible pressure loss.

Previous studies have shown that regions of aortic wall with high WSS correlate with dysregulation of the extracellular matrix and degeneration of the elastic fibers (7).

Van Ooij *et al*. (42), in a recent large 4D flow MRI cross-sectional study (n=571), investigated distinct patterns of WSS on the ascending aorta stratified by aortic valve phenotype and stenosis severity, and demonstrated significant increases of aortic WSS in AS patients compared to controls, subjects with aortic dilatation and BAV patients.

In patients with aortic dilatation and normal valve the vessel diameter is inversely correlated to peak systolic WSS (42) and is associated with slow helix-type flow (30).

The presence of moderate and severe AS, in both TAV and BAV subjects, results in significantly elevated flow velocities, high velocity transvalvular outflow jets, and eccentrically elevated WSS in the ascending aorta (33,42).

Additionally, the increased variability in 3D WSS patterns for patients with AS reflects the heterogeneity of the transvalvular outflow resulting in altered WSS distribution (7).

Flow displacement is the most reliable quantitative parameter used to quantify the eccentricity of the flow jet in the ascending aorta, as demonstrated by Sigovan *et al*. (16).

High degrees of flow displacement have been often

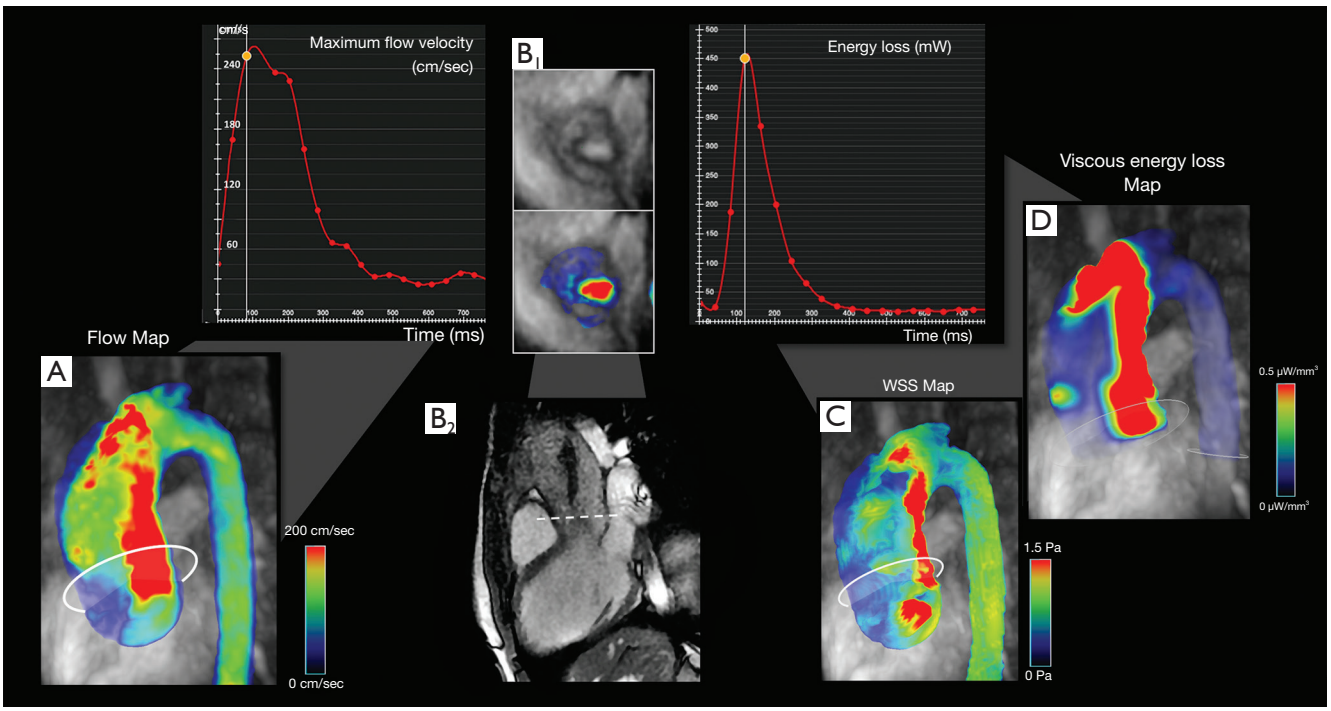

Figure 3 Aortic stenosis. A 45-year-old man with type 0 BAV and aortic valve moderate stenosis. The 4D flow velocity map (A) shows an increased flow velocity at measurement plane (sinus), as specified in the graph above. (B) Three chambers Cine SSFP shows the signal loss of stenotic jet (B2); on the systolic phase contrast images (B1) positioned at the valvular plane (corresponding to the dotted white line on B2) the planimetry of the effective orifice area was calculated as 1.53 cm^2. (C) WSS map and (D) viscous energy loss map describe increased WSS and viscous energy loss along the posterior AscAo wall with similar distribution patterns at systolic peak. The related graph represents the trend of the energy loss at the sinus level, with the maximum value recorded at the systolic peak. BAV, bicuspid aortic valve; WSS, wall shear stress.

observed in AS, and has been shown to correlate well with aortic growth rate, making this parameter another potential risk marker in patients susceptible to valve induced aortic dilatation (37).

4D flow MRI might be a discriminating factor when the echocardiographic grading techniques are discordant (37) and identify significant AS even at low gradient.

Further investigation with a larger population should clarify the potential role of 4D flow MRI derived parameters in prognostic stratification and in depicting the optimal time for surgical repair or valve replacement (33).

Aortic valve regurgitation

The most common causes reported for aortic regurgitation (AR) are bicuspid aortic valve (BAV), infective endocarditis and dilatation of the aortic annulus related to connective tissue disorders (37).

According to 2014 AHA/ACC guidelines, echocardiography is the imaging technique of choice in confirming the presence, severity and aetiology of AR. The assessment of reversed flow during diastole in the aortic arch when compared to the forward systolic flow provides a quick semiquantitative estimate of regurgitant fraction (RF), and the evaluation of LV size and systolic function determines whether there is equilibration of aortic and LV diastolic pressure (43).

CMR is indicated in patients with suboptimal echocardiographic data (class IB) and represents a useful tool in case of discordance between clinical assessment and echocardiographic findings.

Indications for treatment depends on several factors, including presence of symptoms, AR severity, LV dilatation or function impairment (37). More specifically, symptomatic patients with chronic severe AR and patients with no symptoms but LV dysfunction (LVEF <50%) have the

strongest recommendation for surgical intervention (43).

Nowadays, there is no unanimous consensus about the optimal threshold for classifying severe AR by CMR. Based on the measurement of the aortic regurgitant orifice (ARO) and RF it may be classified into mild (RF <20%), moderate (RF: 20–29%, ARO: 0.3–0.5 cm^2) and severe (RF ≥30%, ARO ≥0.5 cm^2), when RF is measured on PC-MRI images acquired at the sino-tubular junction (40).

To this day there is a lack of evidence on literature about the role of 4D flow MRI techniques to assess AR, mostly because the studies have a limited pool of patients.

However recent studies have corroborated the validity of 4D flow MRI compared with echocardiography. Specifically, in 2012, Hsiao *et al*. found a good agreement between CMR 4D flow imaging and echocardiography in evaluating insufficiency in aortic valves (n=5), pulmonary valves (n=11), mitral valves (n=3) and tricuspid valves (n=10), and 4D flow MRI was both highly sensitive (100%) and highly specific (observer 1 =91%; observer 2 =87%) for more than mild valvular regurgitation (44).

Chelu *et al*. have confirmed these findings, through comparison of parameters available for both techniques: ratio between the width of regurgitant jet and of the left ventricle outflow tract, ratio between the length of the regurgitant jet and of the left ventricle, and the presence of reversal flow during diastole at the level of the descending aorta, and using echocardiographic recommendations for grading criteria.

For the detection and grading of AR, 4D PC MRI correlated well with TTE (k =0.73) and all patients with clinically relevant AR were correctly identified by 4D flow MRI (sensitivity: 100%, specificity =98%) (45). The major restriction in both studies is that the comparison between the two techniques is made solely with a qualitative approach. Due to the different methods used to evaluate AR severity, the echocardiographic semi-quantitative one and 4D flow MRI quantitative one, the direct comparison between the two techniques is still challenging.

An improvement in accuracy of direct flow volume quantification by 4D flow MRI, is obtained with the retrospective valve tracking. This approach is very precise and warrants a greater reproducibility, thanks to the capability to dynamically change the three-dimensional position of measurement planes for every time frame, according to the motion of the heart and to the flow direction during the cardiac cycle, an operation that cannot be performed in 2D cine PC sequences (46-48).

A limitation of the technique is need for manual interaction in positioning (or adjusting, if the analysis is semiautomated) of the measurement plane perpendicularly to the inflow direction, which is a time-consuming procedure and might be affected by observer variation (49). However, retrospective valve tracking has found to be reliable for net flow quantification across the aortic valve, with an intraclass correlation coefficient (ICC) of 0.93, P<0.001 for intra-observer results, and an ICC of 0.98, P<0.001 for inter-observer findings (50).

A recent retrospective, observational cohort study showed an excellent correlation even between 4D flow MRI and traditional 2D PC MRI by evaluating forward flow (r=0.826/P<0001), regurgitant flow (r=0.866/P<0001) and regurgitation fraction (r=0.761/P<0001) in patients with varying grades of AR (51).

They also suggested that 4D flow MRI enables us to evaluate other flow variables, such as turbulence or jet diameter, that might improve the AR grading (*Figure 4*).

Although the published work is encouraging for the technique, further research is needed to validate its use as a clinical tool in this pathology.

BAV

BAV is the most common congenital valvular disease. It occurs in 0.5–2% of the general population (52). In patients with BAV, the aortic valve is made of two leaflets, instead of three (52). According to Sievers *et al*., aortic valve phenotypes can be divided into different patterns based on the number of raphes, the spatial position of cusps or raphes and the functional status of the valve. BAV type 0 has equal size cusps and no raphes, type 1 has one raphe and type 2 has 2 raphes. Both type 1 and 2 have non-equal size cusps. Type 1 is described as RL when the fusion involves right and left coronary cusps, RN for the right and non-coronary cusps and LN for the left and non-coronary cusps. In Sievers' study, the prevalent phenotype was type 1 (269, 88%), in particular the RL type (119, 39%); type 0 was very uncommon (21, 7%) and the least represented was type 2 (14, 5%) (53). Other classification systems were proposed by Sabet *et al*. (54), Roberts *et al*. (55) and Angelini *et al*. (56). But Sievers' still remains the most used system/classification (57).

BAV is frequently related to aortic dissection or aneurysm, in fact only 26–35% of BAV are not affected by aortic dilatation (17,58). According to Youssefi *et al*., aortic aneurysms in BAV can be explained by different phenomena: the several molecular disorders affecting the aortic valve

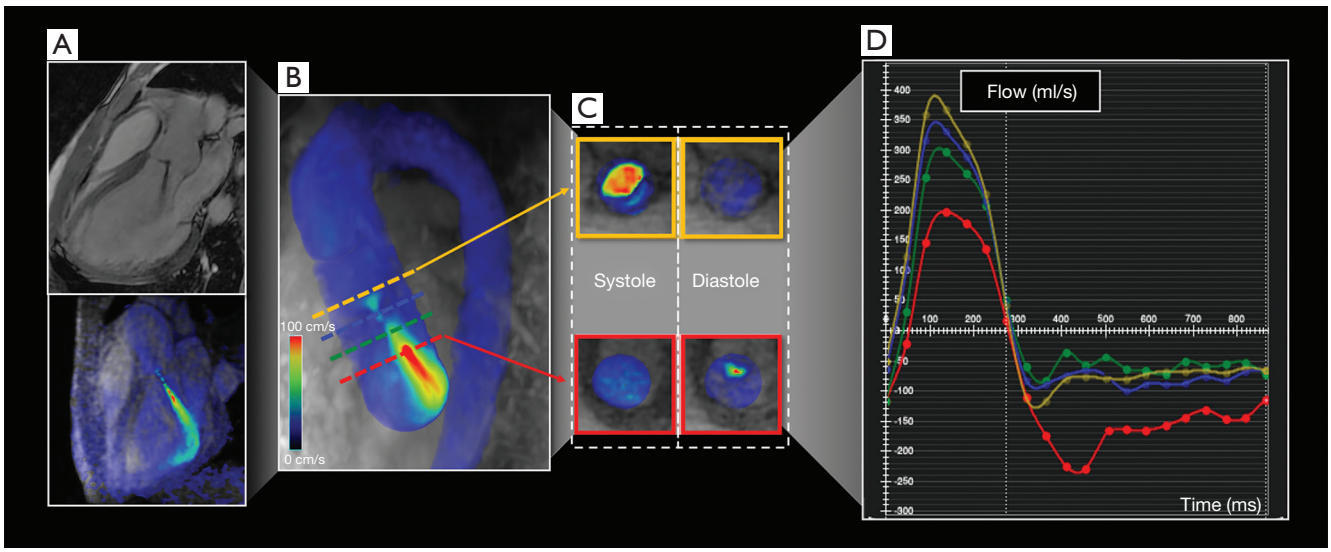

Figure 4 Aortic valve regurgitation. MRI images from a 25-year-old woman with BAV and moderate aortic valve insufficiency. Three chambers cine SSFP (A) shows the aortic regurgitation during diastolic phase (on the top) and with the overlapping bi-dimensional flow image reconstructed from 4D flow dataset (on the bottom). Three-dimensional flow velocity map in diastolic phase (B) and four different axial planes for flow measurements. 4D flow MRI enables the post-hoc hemodynamic analysis at any level along the course of the vessel, as shown in the axial sectional images acquired during peak systolic and diastolic phase (C) acquired above (yellow) and below (red) the valve plane. Graph (D) represents flow-to-time curves measured through the reconstructed axial planes (according to the different colors of image B); the red curve, acquired below the valve plane, better estimates the regurgitant flow. BAV, bicuspid aortic valve.

and the aortic wall (cystic medial degeneration, decrease in fibrillin content and altered activity of metalloproteinases) and turbulent flow, which leads to a haemodynamic stress on the aortic wall and to aortopathy (59,60).

The most frequent site of aneurysm formation seems to be the ascending aorta (59), but dilatation patterns depend on the BAV phenotype (61). RL-type is often related to aortic root and ascending aorta aneurysm (*Figure 5*), while RN-type is more frequently associated with ascending aorta and aortic arch dilatation without the involvement of aortic root (17,62). Rodriguez *et al*. tried to correlate aortic flow patterns with different BAV phenotypes with no severe valvular disease, analyzing the most frequent BAV types (RL and RN-type 1) with 4D-flow. They confirmed that RL types are more likely to develop aortic root dilatation, whereas RN types usually have no or less root involvement. Moreover, they found interesting differences regarding flow characteristics: RL types presented an anterior and right-anterior output flow towards the aortic wall, while RN had a predominant posterior flow, which became right-anterior only in the distal segment of ascending aorta, even if RN types presented a higher variability in flow pattern. Also, RN had a greater jet angle and in-plane rotational flow than RL types. The axial average WSS was higher in RL types in proximal and mid ascending aorta, as compared to RN that showed higher circumferential WSS in mid and distal ascending aorta (17). These results are in line with other studies (30,63,64), but Bissel *et al*. also found a left-handed helical flow in RN-BAV, which was linked to a worse aortopathy, increased aortic diameter, flow angle and WSS values and it was present only in young patients (<26 years old). This left-handed flow was related to a worse prognosis. Furthermore, they observed that BAV patients with aortic stenosis had higher values of WSS and increased WSS eccentricity (65), supporting Hope's retrospective study (which showed a higher annual ascending aortic growth rate in BAV patients with valvular disease) (66) and Barker's study (that associated alteration and heterogeneity of WSS and flow markers with the presence of a retrograde flow) (67).

Another interesting prospective study by Meierhofer *et al*. compared BAV patients with no severe valvular stenosis or insufficiency with a group of tricuspid aortic valve (TAV) controls. They found that in TAV subjects the predominant laminar flow made axial WSS higher that in BAV patients, where the presence of right and left-handed helical flow

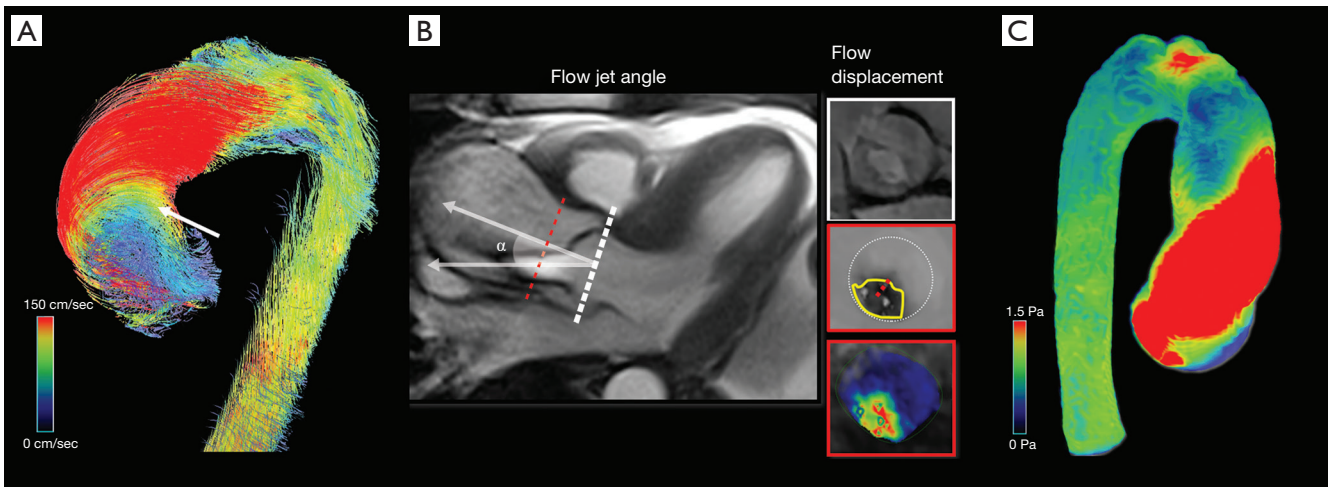

Figure 5 Bicuspid aortic valve. A 33-year-old man with RL-type bicuspid aortic valve, mild aortic valve steno-insufficiency and AscAo dilatation (AscAo maximum diameter =44 mm). Streamlines map (A) shows an increased helicoidal pattern into the AscAo during systole (arrow) due to the flow jet angulation (α), as shown on the three chamber CineMR image (B, left), and increased flow eccentricity, depicted on the axial images of the AscAo (B, right; CineMR in white square and velocity-encoded images in the red squares). WSS Map (C) shows increased systolic WSS on the anterolateral right wall of the dilated portion of AscAo, which reflects the impaired flow pattern caused by the redirection of the outflow jet. WSS, wall shear stress.

determined the increase of circumferential WSS. This stress towards the aortic wall causes a remodeling of the artery (degeneration of extracellular matrix and elastic fibers) and explaining the aneurysm formation (27), thus confirming other studies by Frydrychowicz *et al*. (68).

BAV is also associated to proximal aortic arch dilatation, as it was showed in a study by Dux-Santoy *et al*. They compared BAV patients to TAV controls and found an increased flow eccentricity and rotational flow in the proximal and mid arch in BAV. These characteristics where not found even in dilated TAV. In particular, the altered flow patterns were more frequent in RN phenotype, even though they can also be observed also in RL BAV with valvular stenosis and root dilatation, because of the asymmetrical increase of WSS and heterogeneous aortic wall degeneration (69,70).

BAV patients may benefit from a 4D flow MRI evaluation and CMR follow-ups in order to identify the subjects at risk of rupture or dissection before aortic diameter reaches the cut-off values for surgical treatment.

Aortic aneurysm

According to the joint councils of the Society of Vascular Surgery and the North American Chapter of the International Society for Cardiovascular Surgery, the aneurysm is the permanent focal dilatation of an artery, where the increase in diameter is at least 50% greater than the normal value (71). Aneurysms generation and growth can be explained by Laplace's law, which states that wall tension of a cylinder (the vessel) depends on the pressure inside the cylinder itself and its radius. Therefore when the pressure inside the vessel increases, the wall tension rises (72).

Thoracic aorta dilatation is associated either to congenital diseases related to degeneration of the aortic wall and cystic medial necrosis such as Marfan syndrome (MFS), Ehler Danlos syndrome or BAV, or to acquired pathological conditions like atherosclerosis and hypertension (degenerative etiology). Other rare causes of aneurysm are bacterial infections, Takayasu and Giant cell arteritis (73). Thoracic aorta can be divided into 4 portions: the aortic root (the portion between the valvular annulus and the sinotubular junction, which contains the sinuses of Valsalva, where the coronary arteries originate), the ascending aorta (from the sinotubular junction to the aortic arch), the aortic arch which gives origin to the innominate artery, the left common carotid artery, and the left subclavian artery), and the descending aorta (from the aortic isthmus) which gives rise to paired intercostal arteries from the posterior wall (74,75).

Normal aortic diameter varies with age, sex, body surface area (BSA) and imaging modality. In particular,

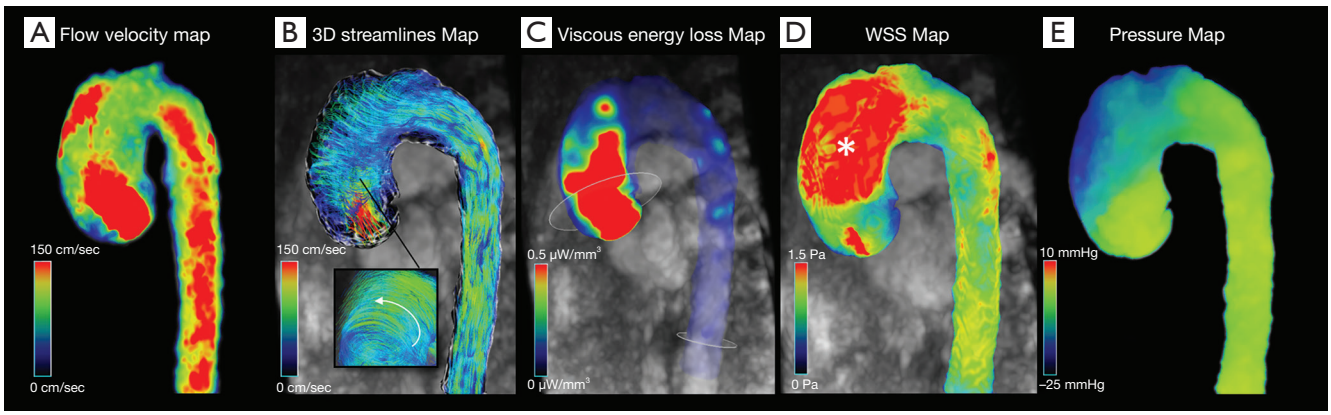

Figure 6 Aortic aneurysm. 4D flow MRI images from a 20-year-old male with AscAo aneurysm and moderate aortic valve insufficiency (AscAo maximum diameter =50 mm, STJ maximum diameter =45 mm). Flow velocity map (A) shows systolic peak flow velocity increased at the center of the aortic root with deceleration through the AscAo. 3D streamlines visualization of systolic blood flow (B) in the thoracic aorta draw a turbulent helicoidal flow pattern along the dilated AscAo during systole; in the black square the rotational streamlines of the turbulent flow are zoomed and visualized with a point of view form the bottom up of the aortic root. Viscous energy loss (C) and WSS (D) maps reconstructed at systolic peak show increased viscous energy loss in the proximal AscAo (red color) and the associated increase of WSS at the downstream aneurysmatic portion of the AscAo (asterix). Pressure gradient is decreased in the aneurysmatic part of the Ao (blue color) during the early systolic phase on the pressure map (E). WSS, wall shear stress.

non-contrast computed tomography (CT) and magnetic resonance (MR) also measure the aortic wall thickness, so measurements can differ by 0.2 to 0.4 cm from those taken with 2D echocardiography (76-79).

Current guidelines assess the risk of progression and dilatation of the aneurysm through periodic diameter measurements and the evaluation of risk factors such as smoking, blood pressure, renal failure, male sex or congenital syndromes and rapidly increasing aortic size. Surgical intervention is recommended when aortic diameter is greater than 5.5 cm (4.5–5 cm in case of MFS, BAV or other genetical disorders) or if the patient is symptomatic or if the growth rate is greater than 0.5 cm/y (59,73,77,80). But aneurysm rupture or dissection can also occur when aortic diameter is within the normal range with an incidence of 5–10% (81,82). As a matter of fact, the risk of rupture is connected to elastin degradation, increase in glycosaminoglycans (GAGs) and in wall permeability. These phenomena are supposedly related to altered aortic hemodynamics (82).

In this scenario, 4D flow MRI can provide useful elements for the qualitative and quantitative evaluation of flow characteristics (such as helicity, WSS or flow jet eccentricity) and allow a precise evaluation of aortic haemodynamics in order to elaborate adequate treatment strategies (*Figure 6*) (34,83,84).

According to the literature, the different morphology of the aneurysms reflects flow characteristics.

Kari *et al*. (85) reported the identification of flow eccentricity and flow compression increasing (constriction of the cross-sectional area constrained by the main systolic jet) in patients with no aortic stenosis or BAV, suggesting the presence of other anathomical and biomechanical aspects that influence aneurysm development (85). Elevated flow eccentricity was linked to high values of WSS which is expected to be determination in long term wall remodeling, rather than rupture which is more closely related to acute events (hypertension peak or blood overload) (84).

Aortic root dilatation mostly affects patients with connective tissue disorders, in particular MFS, in which it leads to aortic root rupture or dissection (86,87). According to the literature, main findings in MFS patients with aortic root dilatation are connected to altered flow patterns and WSS. Some studies conducted on MFS pediatric subjects reported the presence of a local (it involved just a limited region of the vessel) helical flow at the left posterior inner curvature of the ascending aorta, which was correlated to the dilatation of the sinuses of Valsalva (86,88). This helical flow was not encountered by Wang *et al*. who analized flow patterns in elder MFS patients (mean age 30±12). They explained these differences with the progression of the aortic wall dilatation

that results in different degrees of disturbed flow (89). Another common finding was the reduction in both axial and circumferential WSS, associated to an increased WSS eccentricity and a heterogeneous distribution of WSS compared to control groups, with a sort of inverse proportionality between decreasing WSS and increasing aortic diameter (88,89). Furthermore, Geiger *et al.* found a lower peak systolic velocity and a decreased net flow per cycle in MFS patients (86). Applying the technique of 4D pressure mapping to 4D flow MRI, Leidenberger *et al.* found a reduction of aortic wall distensibility and an increased regional pressure gradient at mid-systole in proximal ascending aorta in MFS subjects, which strongly correlates with larger aortic root diameter (81). Interestingly, non-physiological vortex flow was not noticed in the ascending aorta or in the aortic arch, but it was found at the inner curvature of the proximal descending aorta (critical site for type B dissection in MFS), which was not related to aneurysm or dilatation. It has been explained with a reduction in aortic wall distensibility and an increase in positive pressure peak in that region (81,88).

The vortex was associated with a reduction in circumferential WSS at that level (88).

Apart from MFS and BAV syndrome (BAV 4D flow MRI characteristics have been discussed in the respective paragraph), aneurysms based on atherosclerotic aetiology manifest with different flow patterns and characteristics. Hope *et al.* divided patients with ascending aortic aneurysms in several different flow patterns. In the first type, after travelling along the anterior curvature of ascending aorta, part of the flow continued in a retrograde sense in the region of left coronary sinus. The second type was characterised by a helical flow in the center of the aneurysm and circumferential flow in the periphery. In another patient a right-handed helix formed during flow movement towards aortic arch. In the last type, there was a helical flow around the systolic jet in the middle of the aneurysm. They also found a reduction in average velocity in the ascending aorta compared to controls. Unfortunately, the analysis did not show any statistical correlation between diameter and length of the aneurysm and the type of flow pattern, therefore they hoped for long-term and prospective study in order to establish a relationship between different flow patterns and aortic dilatation characteristics (28). Inevitably degenerative ascending aorta aneurysms flow patterns are difficult to standardize, but they often show the presence of helical or vortical flow, retrograde flow and altered velocity or anomalous acceleration (90). Natsume *et al.* analyzed flow characteristics in 82 patients with fusiform and saccular aneurysm of the aortic arch. Vortex flow was present in the ascending aorta (even if not dilated) and inside the aneurysm. Peak and mean WSS were lower compared to control subjects. Another interesting finding was the inverse correlation between the sac depth width ratio and the WSS peak. In particular, they found a similarity between outer curvature saccular aneurysms and fusiform aneurysm in which sac depth width ratio was >0.8 (lower WSS) rather than inner curvature saccular aneurysm with a ratio <0.8 (higher WSS) (91).

High oscillatory shear index (OSI) is a well-known mechanism of atherogenesis and vascular remodelling, similar to low WSS (92). It is also suspected of playing a role in aneurysm initiation and development, as it leads to changes in the vessel wall architecture, such as endothelial cell loss and proliferation of smooth muscle cells (93), which can reduce aortic distensibility.

Several studies have focused on this correlation, and regarding thoracic aorta Burk *et al.* showed the decrease in systolic WSS and increase in OSI in patients with dilated AAo (30), suggesting that low and oscillatory WSS are predisposed to local vessel wall weakening.

In conclusion, there are different flow patterns related to aneurysm aetiology and to the portion of thoracic aorta involved. Aneurysms associated with congenital syndromes often present with similar flow alteration, while atherosclerotic aortic dilatation manifest with different qualitative and quantitative flow characteristics. 4D flow MRI can guide the risk stratification of patients and help to prevent rupture or dissection of the aneurysm at an early stage of the disease.

Coarctation

Aortic coarctation (CoA) accounts for 5% to 7% of all congenital heart disorders, often associated to hypertension, aortic aneurysm, dissection, and aortic insufficiency (94,95).

In this condition, the pressure gradient across the stenosis and the post-stenotic pressure loss are the hemodynamic parameters that most guide the treatment (96). According to clinical guidelines, intervention is recommended when the systolic gradient is higher than 20 mmHg (95). The pressure gradient is commonly measured directly by invasive catheterization or indirectly estimated by TTE. However the first method does not offer accurate information on the aortic dimensions and the second technique lacks the time-resolved and three-

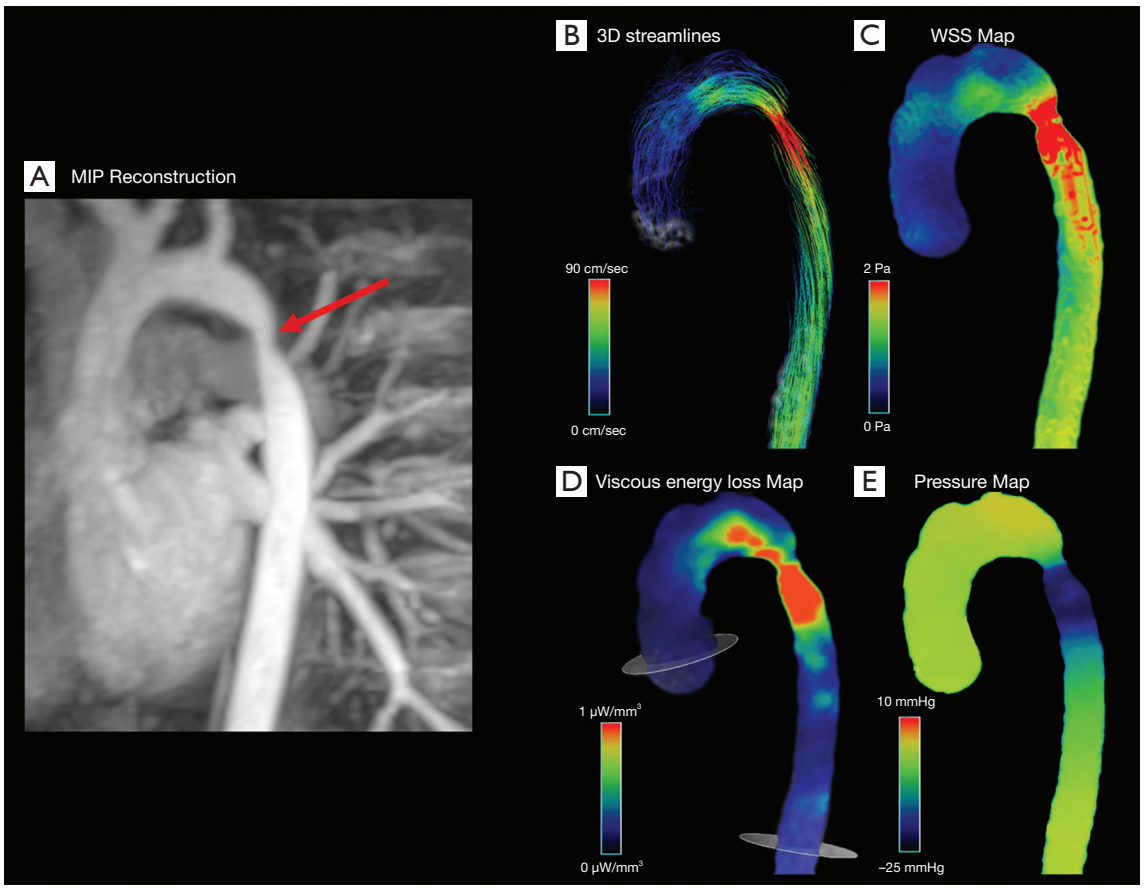

Figure 7 Coarctation. Maximum intensity projection reconstruction of MR Angiography (A) from a 13-year-old female patient with aortic coarctation (arrow). Systolic streamlines (B) and WSS (C) maps describe an increased flow velocity and increased WSS at coarctation site and at the immediately downstream portion of the vessel, respectively. Increased turbulent kinetic energy loss located pre- and post-coarctation site is shown on Viscous Energy Loss map (D), whereas the pressure map during systolic phase (E) highlights pressure drop after the stenosis. WSS, wall shear stress.

dimensional information for the entire thoracic aorta (96).

4D flow MRI allows for, in one acquisition process, the assessment of altered aortic velocity profiles in the thoracic aorta and collateral blood flow (94), which frequently occur to compensate the flow reduction on downstream district.

Hope *et al*. showed that patients with successful surgical repair have normal-appearing velocity profiles across the thoracic aorta. However, the presence of systolic helical flow was noted in the descending thoracic aorta in these patients, and they postulated an association between this abnormal flow and the occurrence of hypertension, a common complication after CoA repair (94).

In CoA patients, the irregular vessel shape with a relevant stenosis can lead to a significant blood deceleration proximal to the narrowing, where the kinetic energy is partially transformed into static pressure energy (*Figure 7*) (94).

Riesenkampff *et al*. compared pressure fields by 4D flow MRI with pressures measured by the catheterization (gold standard) and found a good agreement between the two imaging modalities for 5 different measurement sites along the aorta. For all sites, the correlation coefficients between measures varied between 0.86 and 0.97 ($P<0.001$), suggesting that 4D flow MRI can be used for pressure fields computation as an alternative to invasive diagnostic catheterization, especially in patients with borderline indication for treatment (45).

Furthermore, when the anatomical result after surgery is not optimal, 4D flow MRI could be extremely useful to differentiate between not-significant mild residual narrowing, vascular tortuosity generating turbulent flows

and hemodynamically relevant recurrent CoA (96). The derived hemodynamic parameters (WSS, TKE) calculated by 4D flow MRI could further characterize the prognosis in these patients and therefore help pinpoint the optimal timing of surgical treatment.

Aortic dissection

Aortic dissection, along with intramural hematoma and aneurysm rupture, is part of the spectrum of acute aortic syndromes, a group of life-threatening conditions still difficult to diagnose and manage nowadays.

When the dissection does not involve the ascending aorta (Stanford type B) medical therapy represents the first line treatment and frequent follow-up imaging is required to predict complications.

International Registry of Acute Aortic Dissections data suggest that long-term results of medical management of aortic dissection are still unsatisfactory (97), confirming the need to continue improving the diagnosis and therapeutic management of aortic dissection.

Prophylactic surgical intervention is currently guided by diameter criteria and reserved for patients with severe aortic dilatation (diameter >55 mm for AscAo, or 55 to 60 mm for DesAo, except for patients with connective tissue disorders) (98), although complications frequently occur in aortas with diameter below the threshold for preventative surgery, the so-called aortic size paradox (99).

4D flow MRI appears to be promising for a deeper understanding of the mechanisms leading to early or late complications. In particular, it could refine the selection of those patients who would benefit from preventative surgical intervention (99).

4D flow MRI may offer a qualitative and quantitative flow analysis in both true lumen (TL) and false lumen (FL), their interdependence and competitiveness, combined with an assessment of the pressure effect on the respective walls and, eventually, the risk of rupture.

François *et al*. (100) evaluated alterations in flow patterns using 4D MRI in 12 subjects with thoracic aortic dissection. They encourented primarily laminar flow in the TL, while in the FL they reported complex, abnormal, nonlaminar flow patterns, with the frequent occurrence of systolic retrograde flow. It has been postulated that retrograde flow may be indicative of distal reentry pathways in the FL with higher pressure, which may cause transient obstruction of flow through the TL during systole.

Clough *et al*. (101) confirmed multidirectional and complex blood flow in the FL and reported a significant correlation between the amount of helicity and the rate of false lumen expansion. They have also noted that the position of the dominant entry tear is associated with the area of greatest false lumen expansion. The presence of thrombus was associated with areas of low velocity and complex flow but was not protective from aortic expansion (101).

All of these studies demonstrate the potential predictive role of 4D PC-MRI for risk stratification for rupture in patients with aortic dissection.

Otherwise, Jarvis *et al*. (102) characterized flow alterations in patients with chronic descending aortic dissection (DAD) evaluating directional flow, flow stasis and kinetic energy with 4D flow MRI.

They reported elevated TL reverse flow, TL and FL kinetic energy in patients with DAD having undergone to previous type A surgical repair (n=14), compared to medically managed DAD population (n=6) and healthy controls (n=21), suggesting that complex flow occurring in the residual dissection after ascending aorta surgical repair might be the result of a noncompliant graft, a possible cause of ensuing complications.

Future studies are needed to determine hemodynamic parameters that might help identify patients who could benefit from preventative treatment by TEVAR, help to plan invasive procedures and monitor asymptomatic patients over time.

Post-operative imaging

The interaction between anatomical surgical results and post-operative flow dynamics is a very promising field of interest and has been the object of many studies.

Moreover, many efforts have been oriented to find quantitative flow parameters that might predict late complications and better understanding of the relationship between fluid dynamics and mechanical loads acting on the wall in both of aortic wall and grafts (*Figure 8*).

Among the different surgical techniques for thoracic aorta pathology, the valve-sparing aortic root replacement (VSRR) with reimplantation technique, the so-called David procedure, attracted considerable interest (32).

This technique is a well-established surgical option for the treatment of aortic aneurysms with preserved cusps, as it avoids the need for lifelong anticoagulation therapy.

Recreation of the sinuses of Valsalva during VSRR has been demonstrated to be associated with significantly lower WSS and organized vortical flows at the level of the sinus

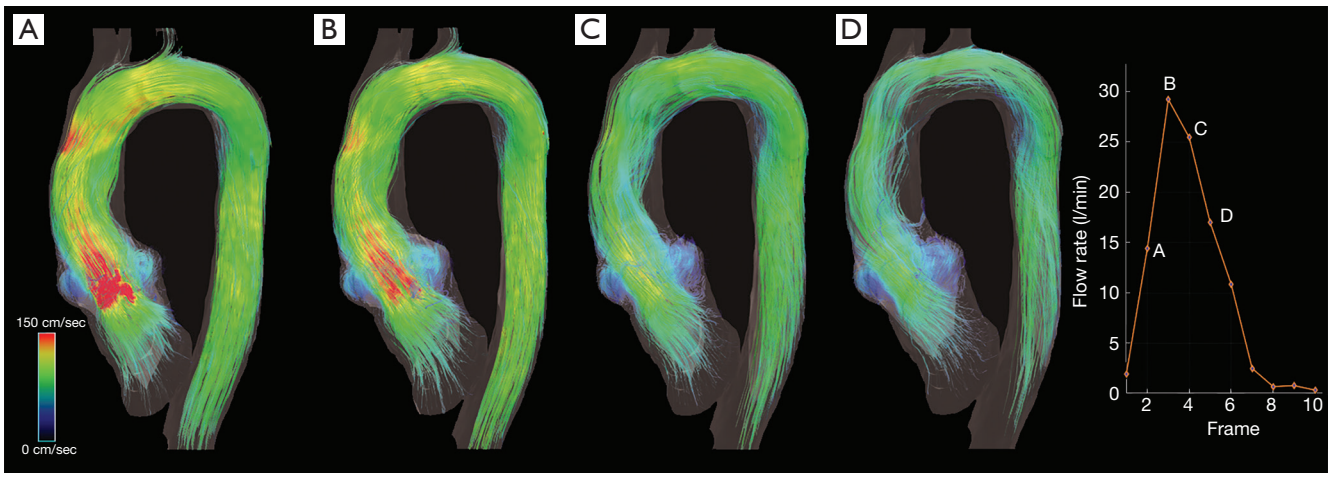

Figure 8 Post-VSRR imaging. 4D flow MRI images from a 37-year-old male patient operated with VSRR and neo-sinus reconstruction. Color encoded streamlines maps shows the flow at systolic peak (A) with increased flow velocity in the aortic root and formation of small organized vortex in the neo-sinus. The operation allowed the restoration of a central laminar flow. The images on the right (B, C and D) demonstrate the progressive deceleration of flow during the following phases and the persistence of the vortices in neo-sinus in diastole.

that are not evident using the straight tube graft (103).

Oechtering *et al*. (104) demonstrated as 4D flow MRI examination revealed disturbed flow patterns distal to aortic root prostheses generated by kinking of the prosthesis itself or at anastomoses. The author concluded that the postoperative altered aortic geometry is correlated with increased secondary flow patterns that are closely linked to WSS changes and increased risk of accelerated vessel wall remodeling and aneurysm growth (105).

The clinical influence of these findings remains at present unclear, and future studies are necessary to clarify their impact on the long-term outcome.

Regarding endovascular treatment, recent studies (106) have highlighted the new role that 4D flow MRI can play in endoleak characterization during endovascular aneurysm repair (EVAR) follow-up, due to the possibility of combining three-dimensional anatomical and velocity information in a single study.

Endoleaks are a common complication following EVAR and although only a small percentage of endoleaks require re-intervention, long-term follow-up is necessary to detect its early or late occurrence.

Currently, CTA is the modality of choice for surveillance of EVAR patients. However CTA imaging may characterize endoleaks only in a static state and generally do not inform on the directionality and velocity of the endoleak flow, especially in the identification of high flow endoleak (106).

Understanding endoleak flow velocities in the aneurysm sac may help determine the risk of rupture (106) and eventually guide the reintervention decision.

Sakata *et al*. (107) showed a superior sensitivity of 4D flow MRI than CTA in discerning endoleaks, and demonstrated that a type II endoleak can be further classified into 2 distinct subtypes according to the flow patterns of the aortic side branches: type IIa (biphasic flow pattern from a branch vessel) and a type IIb (monophasic flow pattern with inflow and outflow branches).

Similarly, 4D flow MRI can provide useful information for follow-up of type B dissection after EVAR (4). However, the use of 4D flow MRI techniques on follow-up imaging of EVAR still has not been fully evaluated, and the majority of the published studies only debates its use on abdominal aorta, so the possible role for the work-up in endovascular treatment of the thoracic aorta is still poorly understood, due to the lack of studies in TEVAR follow-up.

In conclusion, 4D-flow imaging might have a role as the secondary modality during EVAR follow-up after CT/duplex ultrasound for selecting patients who need reintervention, and it may be a clinical alternative to MRA and CTA in patients with renal failure.

Further investigations with larger patient population are needed.

Pediatric application

Up to date there are limited studies exploring the use of 4D

flow MRI in pediatric disease, and most of the literature so far is limited to case reports and series to date.

The main issues are related to the difficult management of these patients, as studies are usually long and children often require sedation, associated costs and technical limitations, such as insufficient temporal resolution to detect short-duration blood flow patterns in children due to high heart rates or the increase of spatial resolution intrinsically required.

The major studies in aortic disease in pediatric population are focused in BAV (108) and Marfan syndrome (109).

Rose *et al*. (108) exploit the highly reproducibility of aortic 4D flow MRI in tracking the progression of the BAV-related aortopathy over a short-term follow-up.

Geiger *et al*. (109) depicted a typical flow pattern in Marfan subjects, characterized by higher incidence of vortex flow in the proximal DescAo and helix flow in the branching point of the left subclavian artery, which could explain the increased risk of type B dissection.

The pediatric population with congenital disease represents perhaps one of the groups who could benefit the most from this non-invasive, radiation-free imaging method, especially in terms of risk stratification and image-guided surgical decisions. However, validation studies with larger population are necessary.

Conclusions

4D flow MRI offers a new comprehensive evaluation of thoracic aorta, which combines morphological and fluid dynamics information, and its clinical application is increasingly expanding. The 4D flow MRI allows today for a more accurate assessment of valves and aortic flows and signals a better understanding of the relationships between altered hemodynamics and progression of vascular disease. These advanced new parameters have the potential to improve characterization of aortic disease beyond simple flow measurements and implement patient outcome prediction, clinical decision-making and personalized treatment.

Acknowledgments

Figure 8 has been edited by Francesco Sturla, with the permission of Biomechanics Group, Department of Electronics, Information and Bioengineering, Politecnico di Milano, Milan, Italy.
Funding: None.

Footnote

Provenance and Peer Review: This article was commissioned by the Guest Editor (Luca Saba) for the series "Advanced Imaging in The Diagnosis of Cardiovascular Diseases" published in *Cardiovascular Diagnosis and Therapy*. The article was sent for external peer review organized by the Guest Editor and the editorial office.

Conflicts of Interest: The authors have completed the ICMJE uniform disclosure form (available at http://dx.doi.org/10.21037/cdt-20-452). The series "Advanced Imaging in the diagnosis of Cardiovascular Diseases" was commissioned by the editorial office without any funding or sponsorship. The authors have no other conflicts of interest to declare.

Ethical Statement: The authors are accountable for all aspects of the work in ensuring that questions related to the accuracy or integrity of any part of the work are appropriately investigated and resolved.

References

1. Dyverfeldt P, Bissell M, Barker AJ, et al. 4D flow cardiovascular magnetic resonance consensus statement. J Cardiovasc Magn Reson 2015;17:72.
2. Garg P, Westenberg JJM, van den Boogaard PJ, et al. Comparison of fast acquisition strategies in whole-heart four-dimensional flow cardiac MR: Two-center, 1.5 Tesla, phantom and in vivo validation study. J Magn Reson Imaging 2018;47:272-81.
3. François CJ, Srinivasan S, Schiebler ML, et al. 4D cardiovascular magnetic resonance velocity mapping of alterations of right heart flow patterns and main pulmonary artery hemodynamics in tetralogy of Fallot. J Cardiovasc Magn Reson 2012;14:16.
4. Azarine A, Garcon P, Stansal A, et al. Four-dimensional

Flow MRI: Principles and Cardiovascular Applications. Radiographics 2019;39:632-48.
5. Markl M, Frydrychowicz A, Kozerke S, et al. 4D flow MRI. J Magn Reson Imaging 2012;36:1015-36.
6. Soulat G, McCarthy P, Markl M. 4D Flow with MRI. Annu Rev Biomed Eng 2020;22:103-26.
7. Sträter A, Huber A, Rudolph J, et al. 4D-Flow MRI: Technique and Applications. Rofo 2018;190:1025-35.
8. Callaghan FM, Kozor R, Sherrah AG, et al. Use of multi-velocity encoding 4D flow MRI to improve quantification of flow patterns in the aorta. J Magn Reson Imaging 2016;43:352-63.
9. Liu J, Dyverfeldt P, Acevedo-Bolton G, et al. Highly accelerated aortic 4D flow MR imaging with variable-density random undersampling. Magn Reson Imaging 2014;32:1012-20.
10. Bollache E, Barker AJ, Dolan RS, et al. k-t accelerated aortic 4D flow MRI in under two minutes: Feasibility and impact of resolution, k-space sampling patterns, and respiratory navigator gating on hemodynamic measurements. Magn Reson Med 2018;79:195-207.
11. Ma LE, Markl M, Chow K, et al. Aortic 4D flow MRI in 2 minutes using compressed sensing, respiratory controlled adaptive k-space reordering, and inline reconstruction. Magn Reson Med 2019;81:3675-90.
12. Stuber M, Botnar RM, Danias PG, et al. Submillimeter three-dimensional coronary MR angiography with real-time navigator correction: comparison of navigator locations. Radiology 1999;212:579-87.
13. Uribe S, Beerbaum P, Sorensen TS, et al. Four-dimensional (4D) flow of the whole heart and great vessels using real-time respiratory self-gating. Magn Reson Med 2009;62:984-92.
14. Elbaz MS, Calkoen EE, Westenberg JJ, et al. Vortex flow during early and late left ventricular filling in normal subjects: quantitative characterization using retrospectively-gated 4D flow cardiovascular magnetic resonance and three-dimensional vortex core analysis. J Cardiovasc Magn Reson 2014;16:78.
15. Gaudino M, Piatti F, Lau C, et al. Aortic flow after valve sparing root replacement with or without neosinuses reconstruction. J Thorac Cardiovasc Surg 2019;157:455-65.
16. Sigovan M, Hope MD, Dyverfeldt P, et al. Comparison of four-dimensional flow parameters for quantification of flow eccentricity in the ascending aorta. J Magn Reson Imaging 2011;34:1226-30.
17. Rodríguez-Palomares JF, Dux-Santoy L, Guala A, et al. Aortic flow patterns and wall shear stress maps by 4D-flow cardiovascular magnetic resonance in the assessment of aortic dilatation in bicuspid aortic valve disease. J Cardiovasc Magn Reson 2018;20:28.
18. Malek AM, Alper SL, Izumo S. Hemodynamic shear stress and its role in atherosclerosis. JAMA 1999;282:2035-42.
19. Guzzardi DG, Barker AJ, van Ooij P, et al. Valve-Related Hemodynamics Mediate Human Bicuspid Aortopathy: Insights From Wall Shear Stress Mapping. J Am Coll Cardiol 2015;66:892-900.
20. Dyverfeldt P, Hope MD, Tseng EE, et al. Magnetic resonance measurement of turbulent kinetic energy for the estimation of irreversible pressure loss in aortic stenosis. JACC Cardiovasc Imaging 2013;6:64-71.
21. Zajac J, Eriksson J, Dyverfeldt P, et al. Turbulent kinetic energy in normal and myopathic left ventricles. J Magn Reson Imaging 2015;41:1021-9.
22. Barker AJ, van Ooij P, Bandi K, et al. Viscous energy loss in the presence of abnormal aortic flow. Magn Reson Med 2014;72:620-8.
23. Binter C, Gotschy A, Sundermann SH, et al. Turbulent Kinetic Energy Assessed by Multipoint 4-Dimensional Flow Magnetic Resonance Imaging Provides Additional Information Relative to Echocardiography for the Determination of Aortic Stenosis Severity. Circ Cardiovasc Imaging 2017;10.
24. Rengier F, Delles M, Eichhorn J, et al. Noninvasive 4D pressure difference mapping derived from 4D flow MRI in patients with repaired aortic coarctation: comparison with young healthy volunteers. Int J Cardiovasc Imaging 2015;31:823-30.
25. Wentland AL, Wieben O, Francois CJ, et al. Aortic pulse wave velocity measurements with undersampled 4D flow-sensitive MRI: comparison with 2D and algorithm determination. J Magn Reson Imaging 2013;37:853-9.
26. Harloff A, Mirzaee H, Lodemann T, et al. Determination of aortic stiffness using 4D flow cardiovascular magnetic resonance - a population-based study. J Cardiovasc Magn Reson 2018;20:43.
27. Meierhofer C, Schneider EP, Lyko C, et al. Wall shear stress and flow patterns in the ascending aorta in patients with bicuspid aortic valves differ significantly from tricuspid aortic valves: a prospective study. Eur Heart J Cardiovasc Imaging 2013;14:797-804.
28. Hope TA, Markl M, Wigstrom L, et al. Comparison of flow patterns in ascending aortic aneurysms and volunteers using four-dimensional magnetic resonance velocity mapping. J Magn Reson Imaging 2007;26:1471-9.
29. Markl M, Draney MT, Miller DC, et al. Time-resolved

three-dimensional magnetic resonance velocity mapping of aortic flow in healthy volunteers and patients after valve-sparing aortic root replacement. J Thorac Cardiovasc Surg 2005;130:456-63.
30. Bürk J, Blanke P, Stankovic Z, et al. Evaluation of 3D blood flow patterns and wall shear stress in the normal and dilated thoracic aorta using flow-sensitive 4D CMR. J Cardiovasc Magn Reson 2012;14:84.
31. Kvitting JP, Ebbers T, Wigstrom L, et al. Flow patterns in the aortic root and the aorta studied with time-resolved, 3-dimensional, phase-contrast magnetic resonance imaging: implications for aortic valve-sparing surgery. J Thorac Cardiovasc Surg 2004;127:1602-7.
32. Galea N, Piatti F, Lau C, et al. 4D flow characterization of aortic blood flow after valve sparing root reimplantation procedure. J Vis Surg 2018;4:95.
33. Garcia J, Barker AJ, Markl M. The Role of Imaging of Flow Patterns by 4D flow MRI in Aortic Stenosis. JACC Cardiovasc Imaging 2019;12:252-66.
34. Burris NS, Hope MD. 4D flow MRI applications for aortic disease. Magn Reson Imaging Clin N Am 2015;23:15-23.
35. Markl M, Wallis W, Strecker C, et al. Analysis of pulse wave velocity in the thoracic aorta by flow-sensitive four-dimensional MRI: reproducibility and correlation with characteristics in patients with aortic atherosclerosis. J Magn Reson Imaging 2012;35:1162-8.
36. Adriaans BP, Westenberg JJM, van Cauteren YJM, et al. Clinical assessment of aortic valve stenosis: Comparison between 4D flow MRI and transthoracic echocardiography. J Magn Reson Imaging 2020;51:472-80.
37. Blanken CPS, Farag ES, Boekholdt SM, et al. Advanced cardiac MRI techniques for evaluation of left-sided valvular heart disease. J Magn Reson Imaging 2018;48:318-29.
38. Minners J, Allgeier M, Gohlke-Baerwolf C, et al. Inconsistent grading of aortic valve stenosis by current guidelines: haemodynamic studies in patients with apparently normal left ventricular function. Heart 2010;96:1463-8.
39. Ha H, Kim GB, Kweon J, et al. Hemodynamic Measurement Using Four-Dimensional Phase-Contrast MRI: Quantification of Hemodynamic Parameters and Clinical Applications. Korean J Radiol 2016;17:445-62.
40. De Rubeis G, Galea N, Ceravolo I, et al. Aortic valvular imaging with cardiovascular magnetic resonance: seeking for comprehensiveness. Br J Radiol 2019;92:20170868.
41. Bahlmann E, Gerdts E, Cramariuc D, et al. Prognostic value of energy loss index in asymptomatic aortic stenosis. Circulation 2013;127:1149-56.
42. van Ooij P, Markl M, Collins JD, et al. Aortic Valve Stenosis Alters Expression of Regional Aortic Wall Shear Stress: New Insights From a 4-Dimensional Flow Magnetic Resonance Imaging Study of 571 Subjects. J Am Heart Assoc 2017;6:e005959.
43. Nishimura RA, Otto CM, Bonow RO, et al. 2014 AHA/ACC Guideline for the Management of Patients With Valvular Heart Disease: a report of the American College of Cardiology/American Heart Association Task Force on Practice Guidelines. Circulation 2014;129:e521-643.
44. Hsiao A, Lustig M, Alley MT, et al. Evaluation of valvular insufficiency and shunts with parallel-imaging compressed-sensing 4D phase-contrast MR imaging with stereoscopic 3D velocity-fusion volume-rendered visualization. Radiology 2012;265:87-95.
45. Chelu RG, van den Bosch AE, van Kranenburg M, et al. Qualitative grading of aortic regurgitation: a pilot study comparing CMR 4D flow and echocardiography. Int J Cardiovasc Imaging 2016;32:301-7.
46. Roes SD, Hammer S, van der Geest RJ, et al. Flow assessment through four heart valves simultaneously using 3-dimensional 3-directional velocity-encoded magnetic resonance imaging with retrospective valve tracking in healthy volunteers and patients with valvular regurgitation. Invest Radiol 2009;44:669-75.
47. Westenberg JJ, Roes SD, Ajmone Marsan N, et al. Mitral valve and tricuspid valve blood flow: accurate quantification with 3D velocity-encoded MR imaging with retrospective valve tracking. Radiology 2008;249:792-800.
48. She HL, Roest AA, Calkoen EE, et al. Comparative Evaluation of Flow Quantification across the Atrioventricular Valve in Patients with Functional Univentricular Heart after Fontan's Surgery and Healthy Controls: Measurement by 4D Flow Magnetic Resonance Imaging and Streamline Visualization. Congenit Heart Dis 2017;12:40-8.
49. Kamphuis VP, van der Palen RLF, de Koning PJH, et al. In-scan and scan-rescan assessment of LV in- and outflow volumes by 4D flow MRI versus 2D planimetry. J Magn Reson Imaging 2018;47:511-22.
50. Crandon S, Elbaz MSM, Westenberg JJM, et al. Clinical applications of intra-cardiac four-dimensional flow cardiovascular magnetic resonance: A systematic review. Int J Cardiol 2017;249:486-93.
51. Alvarez A, Martinez V, Pizarro G, et al. Clinical use of 4D flow MRI for quantification of aortic regurgitation. Open Heart 2020;7:e001158.
52. Siu SC, Silversides CK. Bicuspid aortic valve disease. J Am

Coll Cardiol 2010;55:2789-800.
53. Sievers HH, Schmidtke C. A classification system for the bicuspid aortic valve from 304 surgical specimens. J Thorac Cardiovasc Surg 2007;133:1226-33.
54. Sabet HY, Edwards WD, Tazelaar HD, et al. Congenitally bicuspid aortic valves: a surgical pathology study of 542 cases (1991 through 1996) and a literature review of 2,715 additional cases. Mayo Clin Proc 1999;74:14-26.
55. Roberts WC. The congenitally bicuspid aortic valve. A study of 85 autopsy cases. Am J Cardiol 1970;26:72-83.
56. Angelini A, Ho SY, Anderson RH, et al. The morphology of the normal aortic valve as compared with the aortic valve having two leaflets. J Thorac Cardiovasc Surg 1989;98:362-7.
57. Ridley CH, Vallabhajosyula P, Bavaria JE, et al. The Sievers Classification of the Bicuspid Aortic Valve for the Perioperative Echocardiographer: The Importance of Valve Phenotype for Aortic Valve Repair in the Era of the Functional Aortic Annulus. J Cardiothorac Vasc Anesth 2016;30:1142-51.
58. Petersen J, Sequeira-Gross T, Naito S, et al. Aortic valve-related aortopathy: assessing optimal timing of surgical intervention. Expert Rev Cardiovasc Ther 2019;17:753-61.
59. Youssefi P, Sharma R, Figueroa CA, et al. Functional assessment of thoracic aortic aneurysms - the future of risk prediction? Br Med Bull 2017;121:61-71.
60. Edlin J, Youssefi P, Bilkhu R, et al. Haemodynamic assessment of bicuspid aortic valve aortopathy: a systematic review of the current literature. Eur J Cardiothorac Surg 2019;55:610-7.
61. Michelena HI, Prakash SK, Della Corte A, et al. Bicuspid aortic valve: identifying knowledge gaps and rising to the challenge from the International Bicuspid Aortic Valve Consortium (BAVCon). Circulation 2014;129:2691-704.
62. Della Corte A, Bancone C, Dialetto G, et al. The ascending aorta with bicuspid aortic valve: a phenotypic classification with potential prognostic significance. Eur J Cardiothorac Surg 2014;46:240-7; discussion 247.
63. Mahadevia R, Barker AJ, Schnell S, et al. Bicuspid aortic cusp fusion morphology alters aortic three-dimensional outflow patterns, wall shear stress, and expression of aortopathy. Circulation 2014;129:673-82.
64. Hope MD, Hope TA, Crook SE, et al. 4D flow CMR in assessment of valve-related ascending aortic disease. JACC Cardiovasc Imaging 2011;4:781-7.
65. Bissell MM, Hess AT, Biasiolli L, et al. Aortic dilation in bicuspid aortic valve disease: flow pattern is a major contributor and differs with valve fusion type. Circ Cardiovasc Imaging 2013;6:499-507.
66. Hope MD, Wrenn J, Sigovan M, et al. Imaging biomarkers of aortic disease: increased growth rates with eccentric systolic flow. J Am Coll Cardiol 2012;60:356-7.
67. Barker AJ, Lanning C, Shandas R. Quantification of hemodynamic wall shear stress in patients with bicuspid aortic valve using phase-contrast MRI. Ann Biomed Eng 2010;38:788-800.
68. Frydrychowicz A, Berger A, Russe MF, et al. Time-resolved magnetic resonance angiography and flow-sensitive 4-dimensional magnetic resonance imaging at 3 Tesla for blood flow and wall shear stress analysis. J Thorac Cardiovasc Surg 2008;136:400-7.
69. Dux-Santoy L, Guala A, Teixido-Tura G, et al. Increased rotational flow in the proximal aortic arch is associated with its dilation in bicuspid aortic valve disease. Eur Heart J Cardiovasc Imaging 2019;20:1407-17.
70. Lorenz R, Bock J, Barker AJ, et al. 4D flow magnetic resonance imaging in bicuspid aortic valve disease demonstrates altered distribution of aortic blood flow helicity. Magn Reson Med 2014;71:1542-53.
71. Evans GH, Stansby G, Hamilton G. Suggested standards for reporting on arterial aneurysms. J Vasc Surg 1992;15:456.
72. Basford JR. The Law of Laplace and its relevance to contemporary medicine and rehabilitation. Arch Phys Med Rehabil 2002;83:1165-70.
73. Nataf P, Lansac E. Dilation of the thoracic aorta: medical and surgical management. Heart 2006;92:1345-52.
74. Baliga RR, Nienaber CA, Bossone E, et al. The role of imaging in aortic dissection and related syndromes. JACC Cardiovasc Imaging 2014;7:406-24.
75. Cohen RG, Elsayed RS, Bowdish ME. Surgery for Diseases of the Aortic Root. Cardiol Clin 2017;35:321-9.
76. Goldfinger JZ, Halperin JL, Marin ML, et al. Thoracic aortic aneurysm and dissection. J Am Coll Cardiol 2014;64:1725-39.
77. Hiratzka LF, Bakris GL, Beckman JA, et al. 2010 ACCF/AHA/AATS/ACR/ASA/SCA/SCAI/SIR/STS/SVM guidelines for the diagnosis and management of patients with Thoracic Aortic Disease: a report of the American College of Cardiology Foundation/American Heart Association Task Force on Practice Guidelines, American Association for Thoracic Surgery, American College of Radiology, American Stroke Association, Society of Cardiovascular Anesthesiologists, Society for Cardiovascular Angiography and Interventions, Society of Interventional Radiology, Society of Thoracic

Surgeons, and Society for Vascular Medicine. Circulation 2010;121:e266-369.
78. Beck L, Mohamed AA, Strugnell WE, et al. MRI measurements of the thoracic aorta and pulmonary artery. J Med Imaging Radiat Oncol 2018;62:64-71.
79. Wolak A, Gransar H, Thomson LE, et al. Aortic size assessment by noncontrast cardiac computed tomography: normal limits by age, gender, and body surface area. JACC Cardiovasc Imaging 2008;1:200-9.
80. Gökalp AL, Takkenberg JJM. Decision-Making in Thoracic Aortic Aneurysm Surgery-Clinician and Patient View. Semin Thorac Cardiovasc Surg 2019;31:638-42.
81. Leidenberger T, Gordon Y, Farag M, et al. Imaging-Based 4D Aortic Pressure Mapping in Marfan Syndrome Patients: A Matched Case-Control Study. Ann Thorac Surg 2020;109:1434-40.
82. Campobasso R, Condemi F, Viallon M, et al. Evaluation of Peak Wall Stress in an Ascending Thoracic Aortic Aneurysm Using FSI Simulations: Effects of Aortic Stiffness and Peripheral Resistance. Cardiovasc Eng Technol 2018;9:707-22.
83. Stankovic Z, Allen BD, Garcia J, et al. 4D flow imaging with MRI. Cardiovasc Diagn Ther 2014;4:173-92.
84. Condemi F, Campisi S, Viallon M, et al. Relationship Between Ascending Thoracic Aortic Aneurysms Hemodynamics and Biomechanical Properties. IEEE Trans Biomed Eng 2020;67:949-56.
85. Kari FA, Kocher N, Beyersdorf F, et al. Four-dimensional magnetic resonance imaging-derived ascending aortic flow eccentricity and flow compression are linked to aneurysm morphologydagger. Interact Cardiovasc Thorac Surg 2015;20:582-7; discussion 587-8.
86. Geiger J, Arnold R, Herzer L, et al. Aortic wall shear stress in Marfan syndrome. Magn Reson Med 2013;70:1137-44.
87. Ammash NM, Sundt TM, Connolly HM. Marfan syndrome-diagnosis and management. Curr Probl Cardiol 2008;33:7-39.
88. van der Palen RL, Barker AJ, Bollache E, et al. Altered aortic 3D hemodynamics and geometry in pediatric Marfan syndrome patients. J Cardiovasc Magn Reson 2017;19:30.
89. Wang HH, Chiu HH, Tseng WY, et al. Does altered aortic flow in marfan syndrome relate to aortic root dilatation? J Magn Reson Imaging 2016;44:500-8.
90. Weigang E, Kari FA, Beyersdorf F, et al. Flow-sensitive four-dimensional magnetic resonance imaging: flow patterns in ascending aortic aneurysms. Eur J Cardiothorac Surg 2008;34:11-6.
91. Natsume K, Shiiya N, Takehara Y, et al. Characterizing saccular aortic arch aneurysms from the geometry-flow dynamics relationship. J Thorac Cardiovasc Surg 2017;153:1413-20.e1.
92. Peiffer V, Sherwin SJ, Weinberg PD. Does low and oscillatory wall shear stress correlate spatially with early atherosclerosis? A systematic review. Cardiovasc Res 2013;99:242-50.
93. Koullias G, Modak R, Tranquilli M, et al. Mechanical deterioration underlies malignant behavior of aneurysmal human ascending aorta. J Thorac Cardiovasc Surg 2005;130:677-83.
94. Hope MD, Meadows AK, Hope TA, et al. Clinical evaluation of aortic coarctation with 4D flow MR imaging. J Magn Reson Imaging 2010;31:711-8.
95. Riesenkampff E, Fernandes JF, Meier S, et al. Pressure fields by flow-sensitive, 4D, velocity-encoded CMR in patients with aortic coarctation. JACC Cardiovasc Imaging 2014;7:920-6.
96. Rengier F, Delles M, Eichhorn J, et al. Noninvasive pressure difference mapping derived from 4D flow MRI in patients with unrepaired and repaired aortic coarctation. Cardiovasc Diagn Ther 2014;4:97-103.
97. Evangelista A, Isselbacher EM, Bossone E, et al. Insights From the International Registry of Acute Aortic Dissection: A 20-Year Experience of Collaborative Clinical Research. Circulation 2018;137:1846-60.
98. Erbel R, Aboyans V, Boileau C, et al. 2014 ESC Guidelines on the diagnosis and treatment of aortic diseases: Document covering acute and chronic aortic diseases of the thoracic and abdominal aorta of the adult. The Task Force for the Diagnosis and Treatment of Aortic Diseases of the European Society of Cardiology (ESC). Eur Heart J 2014;35:2873-926.
99. Adriaans BP, Wildberger JE, Westenberg JJM, et al. Predictive imaging for thoracic aortic dissection and rupture: moving beyond diameters. Eur Radiol 2019;29:6396-404.
100. François CJ. Noninvasive imaging workup of patients with vascular disease. Surg Clin North Am 2013;93:741-60, vii.
101. Clough RE, Waltham M, Giese D, et al. A new imaging method for assessment of aortic dissection using four-dimensional phase contrast magnetic resonance imaging. J Vasc Surg 2012;55:914-23.
102. Jarvis K, Pruijssen JT, Son AY, et al. Parametric Hemodynamic 4D flow MRI Maps for the Characterization of Chronic Thoracic Descending Aortic Dissection. J Magn Reson Imaging 2020;51:1357-68.

103. Galea N, Piatti F, Sturla F, et al. Novel insights by 4D Flow imaging on aortic flow physiology after valve-sparing root replacement with or without neosinuses. Interact Cardiovasc Thorac Surg 2018;26:957-64.
104. Oechtering TH, Sieren MM, Hunold P, et al. Time-resolved 3-dimensional magnetic resonance phase contrast imaging (4D flow MRI) reveals altered blood flow patterns in the ascending aorta of patients with valve-sparing aortic root replacement. J Thorac Cardiovasc Surg 2020;159:798-810.e1.
105. Oechtering TH, Sieren M, Schubert K, et al. In vitro 4D flow MRI evaluation of aortic valve replacements reveals disturbed flow distal to biological but not to mechanical valves. J Card Surg 2019;34:1452-7.
106. Hope TA, Zarins CK, Herfkens RJ. Initial experience characterizing a type I endoleak from velocity profiles using time-resolved three-dimensional phase-contrast MRI. J Vasc Surg 2009;49:1580-4.
107. Sakata M, Takehara Y, Katahashi K, et al. Hemodynamic Analysis of Endoleaks After Endovascular Abdominal Aortic Aneurysm Repair by Using 4-Dimensional Flow-Sensitive Magnetic Resonance Imaging. Circ J 2016;80:1715-25.
108. Rose MJ, Jarvis KB, Barker AJ, et al. Evaluating the disease progression of pediatric bicuspid aortic valve patients using 4D flow MRI data. Journal of Cardiovascular Magnetic Resonance 2016;18:P170.
109. Geiger J, Markl M, Herzer L, et al. Aortic flow patterns in patients with Marfan syndrome assessed by flow-sensitive four-dimensional MRI. J Magn Reson Imaging 2012;35:594-600.

Cite this article as: Catapano F, Pambianchi G, Cundari G, Rebelo J, Cilia F, Carbone I, Catalano C, Francone M, Galea N. 4D flow imaging of the thoracic aorta: is there an added clinical value? Cardiovasc Diagn Ther 2020;10(4):1068-1089. doi: 10.21037/cdt-20-452

